RSC Advances

PAPER

View Article Online
View Journal | View Issue

Cite this: *RSC Adv.*, 2020, **10**, 36378

Preparing dangling bonds by nanoholes on graphene oxide nanosheets and their enhanced magnetism†

Juan Li, ‡ Rongli Cui,‡ Yanan Chang, Huan Huang, Xihong Guo, Jiahao Wang, Ru Liu, Kui Chen, Jianglong Kong, Gengmei Xing* and Baoyun Sun *

Received 8th July 2020
Accepted 24th September 2020

DOI: 10.1039/d0ra05945e

rsc.li/rsc-advances

The effects of dangling bonds on the magnetic properties of graphene oxide (GO) were studied experimentally by creating nanoholes on GO nanosheets. GO with more nanoholes (MHGO) and less nanoholes (LHGO) on graphene oxide nanosheets were synthesized. Results showed that nanoholes brought new dangling bonds for GO and the increase of the dangling bonds on GO could be adjusted by the amounts of the nanoholes on GO. The magnetism of GO was enhanced with increased density of nanoholes on GO (MHGO > LHGO > GO). Furthermore, the increased dangling bonds induced magnetic coupling between the spin units and so converted paramagnetism GO to ferromagnetism (MHGO, LHGO). The easy generation and adjustment of GO dangling bonds by nanoholes on GO nanosheets will promote the applications of GO.

Introduction

Graphene, as a two-dimensional, atomic-scale, hexagonal lattice in which one atom forms each vertex, has attracted significant attention due to its unique electronic, optical, thermal, mechanical and chemical properties, *etc.*[1–3] Graphene has a lot of possible applications in various fields like batteries, sensors, solar panels, electronics and more.[4] Taking advantage of magnetism of graphene is of particular interest since it could open up a new way to design spintronic devices.[5–8]

Ideal graphene is intrinsically nonmagnetic due to a delocalized π bonding network but the chemical structures of graphene could be changed for its application into the different fields by oxidation, chemical doping and so on.[9–11] All the changes of the graphene chemical structures will break of the perfect structure of the π bonding network.[12] In the other words, the chemical processes happened on the graphene enriched the point defects on the edge of graphene,[13,14] such as vacancies,[15,16] zigzag edges,[17] sp^3 functionalization.[18] Moreover, these defects directly changed the electronic status and properties of graphene while the magnetic properties which is the most closely related to the electronic status altered intensely in electronic changed process.[5,19–21] G. Z. Magda *et al.*[17] and L. Salemi *et al.*[22] adjusted the both electronic and magnetic properties of graphene nanostructures by controlling the edges of graphene nanoribbons. Tao Tang *et al.* modified hydroxyl groups on the GO sheets.[23] Takaaki Taniguchi *et al.*[24] used the photo reduced graphene oxide. Kousik Bagani *et al.*[25] also reported the random epoxy groups in the native GO to investigate the relationship between the magnetization of the GO sheet and the defects of hydroxyl groups, C–H bonding, carbon vacancies[24] and epoxy groups[25] on the graphene nanosheets. Blonski Piotr *et al.* verified that N-doping GO had high magnetization of *ca.* 1.66 emu g^{-1}.[26] Among all the chemical methods to change the graphene's nanostructures, chemical groups or heteroatoms were introduced.[27–30] Holey graphene (HG) is a novel graphene structure with amounts of nanopores on the conjugated carbon surface.[13,14,31–33] HG not only retains the excellent properties of graphene, but also exhibits enriched edge and localization effects. Therefore, HG has potential applications in energy storage, gas separation, and magnetic and electronic devices.[34–38] Especially, creating nanoholes on the graphene carried in no other elements in the graphene samples and so suitable to investigate the effects of chemical defects on electronic magnetic properties of graphene.

Where were nanoholes on the GO nanosheets, there were many dangling bonds which are unsatisfied valences on immobilized carbon atoms.[39] In this work, nanoholes were made on the graphene and the different amounts of the dangling bonds were adjusted by controlling the density of nanoholes on the graphene nanosheets. GO with more nanoholes on the graphene oxide nanosheets (MHGO) and GO with less nanoholes on the graphene oxide nanosheets (LHGO) were synthesized, respectively. The generation of dangling bonds and regulation of graphene electronic magnetic properties by

CAS Key Laboratory for Biomedical Effects of Nanomaterial & Nanosafety, Institute of High Energy Physics, Chinese Academy of Science (CAS), Beijing 100049, China. Fax: +86 10 88233595; Tel: +86 10 88233595

† Electronic supplementary information (ESI) available. See DOI: 10.1039/d0ra05945e

‡ These authors contributed equally to this work.

creating nanoholes on GO provide a very convenient method for the development of graphene-based electromagnetic materials.

Experimental

Materials

Natural graphite power (99.9%, Qingdao Hensen Graphite Co., Ltd), HNO_3 (BV-III) was purchased from Beijing Chemical Reagent Research Institute Co., Ltd. All of the other chemicals were purchased from Sinopharm Chemical Reagent Co., Ltd. Deionized (DI) water obtained from a Millipore water purification system was employed in all experiments.

Preparation of GO

GO was prepared according to the modified Hummer's method.[3] Briefly, graphite (0.25 g) was added to concentrated H_2SO_4 (11 mL) at 0 °C. Then, $KMnO_4$ (0.75 g) was added gradually at lower than 20 °C with stirring and kept for 5 h. After that, the reaction system was transferred to a 35 °C water bath for 30 min. Then, 12 mL H_2O was added slowly to the above solution to keep the temperature below 100 °C. After stirring for 30 min, DI water (30 mL) was added to terminate the reaction. Then, H_2O_2 (2 mL, 30%) was added to remove unreacted $KMnO_4$. The mixture was centrifuged and washed with 5% HCl solution and DI water for 3 times, respectively. The obtained brown precipitation was dispersed in DI water through sonication for 60 min and then centrifuged at 12 500 rpm for 30 min, and the supernatant was collected and dried by freeze drying. This product was the prepared GO sample.

Preparation of holey graphene oxide (HGO)

HGO was prepared according to a solution method. Briefly, 10 mg as-prepared GO was dispersed in 10 mL 30% H_2O_2 by sonication and then heated at 100 °C for 2 h and 2.5 h respectively. The as-prepared HGO was purified by centrifugation and washed by DI water for 3 times to remove the residual H_2O_2. Then, the precipitate was dried by freeze-drying. The HGO reacted for 2 h and 2.5 h were marked as LHGO and MHGO for the generation of less nanoholes and more nanoholes on GO nanosheets, respectively. According to the precise control of reaction time, the amount of nanoholes on GO nanosheets could be controlled.

Characterization

The ESR measurements were operated at about 9.1 GHz microwave frequency, 100 kHz field modulation frequency, and at 22 °C. To measure ESR spectra of a series of GO solid samples, the powder of about 20 mg samples was filled in 5 mm ESR tubes. The ESR signals were obtained using 1 mW incident microwave power. The g value was calibrated by using an external marker.

Magnetization measurements of the GO and HGO samples were performed using a physical property measurements system (PPMS) equipped with a vibrating sample magnetometer (VSM) from Quantum Design, USA. Hysteresis loops were measured in the temperature range from 5 to 300 K under static external magnetic fields ranging from −50 to +50 kOe. Temperature profiles of the mass magnetic susceptibility, χ_{mass}, were recorded in a sweep mode in the temperature range from 5 to 300 K in a field of 1 kOe after cooling in a field of 1 kOe. All the solid samples were obtained by freeze drying, and about 20 mg of each dry powder was sealed in a capsule with negligible magnetism.

All magnetic resonance experiments were carried out on a 4.7 T/30 cm Bruker Biospec scanner (Ettlingen, Germany). The longitudinal relaxation time (T_1) measurements were performed with an inversion-recovery spin echo imaging sequence.

Atomic force microscopy (AFM) images were characterized by using a scanning probe microscope (Bruker, Dimension Edge), operated at tapping mode. X-ray photoelectron spectroscopy (XPS) analysis was performed on AXIS-Ultra instrument from Kratos Analytical with monochromatic Al Kα radiation ($h\nu$ = 1486.6 eV). Fourier transform infrared (FTIR) spectra were recorded with Thermo Scientific Nicolet iN10 MX. UV-vis absorption spectra were obtained by a UV-vis-NIR spectrophotometer (Aglient Technologies, Carry 5000). Raman spectra were recorded on a Microscopic confocal Raman microscope (Jobin Yvon, LabRam ARAMIS), using a 532 nm laser beam. The residual metal content in the GO, LHGO, and MHGO samples was analyzed by inductively coupled plasma mass spectrometry (ICP-MS) (PerkinElmer, Nexlon 300D).

Results and discussion

AFM was used to characterize the morphologies of as-prepared samples. The samples were first deposited on new cleaved mica surfaces by corresponding aqueous dispersions and then dried in a vacuum at room temperature before AFM studies. As shown in Fig. 1, the height of GO and HGO was both about 1 nm, indicating the nanosheets of GO and HGO were single layer. GO showed a smooth and clean surface (Fig. 1a). In contrast, the obviously varied density of nanoholes were observed in the GO planes and denominated LHGO (Fig. 1b, 2.5 nanoholes per 100 square nanometers) and MHGO (Fig. 1c, 3.5–4.5 nanoholes per 100 square nanometers). This indicated that the number of nanoholes on the GO nanosheet could be controlled by precisely controlling the reaction conditions (see the Experimental section). The size of nanosheets of LHGO and MHGO had not changed, but the average sizes of the nanoholes in the surface of LHGO and MHGO were 9–10 nm and 11–12 nm, respectively. Particularly, nanoholes greatly increased the edge structure of HGO, and MHGO had more edge structures compared to LHGO due to the increased size and density of nanoholes on the nanosheets of GO. All of the change was resulted by simply extending the etching condition. In the process, dangling bonds present at the edge of nanoholes. Moreover, extending the reaction time could enhance the degree of etching, and so enlarging the nanohole size and increasing the amount of nanoholes on GO. Since the dangling bonds have an important contribution to the edge magnetism of graphene,[39] could the number of dangling bonds of GO be controlled by the size and density of nanoholes on the nanosheets and so adjust and enhance the magnetism of GO?

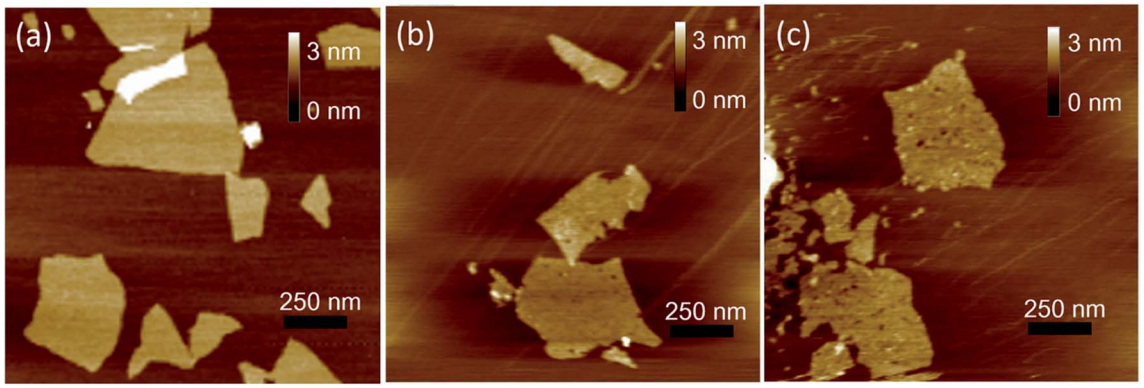

Fig. 1 AFM images of as-prepared GO (a), LHGO (b) and MHGO (c) nanosheets, respectively.

Electron spin resonance (ESR) were used to detect unpaired electrons *i.e.* dangling bonds in materials from both qualitative and quantitative aspects.[40,41] The ESR signal intensity and the spin counts per mg of as-prepared solid samples were detected by the protocol in the section of Characterization. As shown in Fig. 2a, the same single, intense, and sharp ESR signal wave at around 337–338 mT was found in the ESR magnetic field, indicating ESR signals of GO, LHGO and MHGO originating from the unpaired electrons trapped on carbon vacancies, which also provides the direct evidence for the existence of dangling bonds on edge of GO. Since the ESR signal intensity can quantify the unpaired electrons, that is, quantify the dangling bonds, and the unit quality signal intensity of as-prepared samples increased with the increased size and density of nanoholes on GO (MHGO > LHGO > GO) (Fig. 2b), so dangling bonds are mainly from the edge of nanoholes. More importantly, the MHGO sample had the most dangling bonds per mg, followed by LHGO, and finally the GO, indicating the number of dangling bonds could be adjusted by controlling the nanoholes in the basal of GO, which could be realized by precise adjusting reaction time and temperature.

Because the observed ESR signal is assigned to the unpaired electrons localized on carbon vacancies which generate magnetic moments, the magnetic properties of as-prepared GO, LHGO, and MHGO were studied with a physical property measurement system (PPMS) equipped with a vibrating sample magnetometer (VSM).[42,43] In order to exclude the effect of 3d metal impurities on the magnetic properties of as-prepared samples, ICP-MS was employed. The total concentration of Fe, Co, Ni and Mn as the main magnetic impurities was below 70 ppm (see Table S1 in ESI†), thence the total χ_{mass} of Fe, Co, Ni and Mn was estimated to 2 orders smaller than as-prepared GO, SGO, and DGO in a 1 kOe field (Fig. 3 and 4), and so their contributions to magnetism could be negligible.[26] As shown in Fig. 3a, the temperature evolution of χ_{mass} measured for the GO sample obeyed the Curie law $\chi = C/T$. Insert is the corresponding $1/\chi$–T curve, which is a line and so indicates the purely Curie-like paramagnetism of GO. No significant ferromagnetic signal is observed in the M–H curve even at 5 K (Fig. 3b), also indicating that the GO sample is paramagnetic. The saturation magnetization Ms of GO is about 0.14 emu g^{-1} which is similar to the value reported.[44]

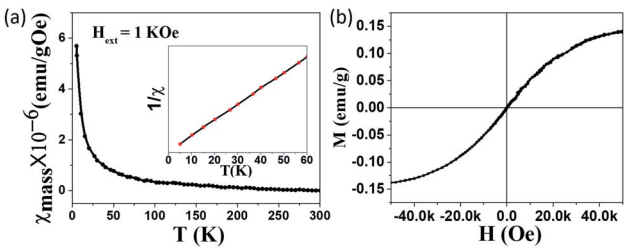

Fig. 3 Magnetic properties of GO measured by PPMS. (a) Typical χ–T curve measured from 5 to 300 K under the extra field H = 1 kOe. Inset is the corresponding $1/\chi$–T curve. (b) M–H curve measured at 5 K.

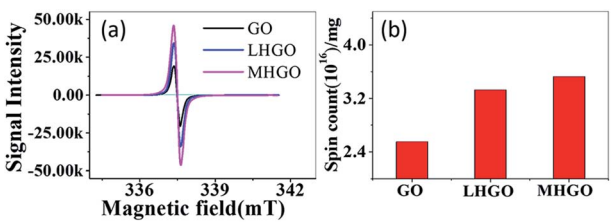

Fig. 2 (a) ESR spectra for solid-state GO, LHGO and MHGO obtained on an X-band spectrometer. (b) The ESR signal intensity for GO, LHGO and MHGO.

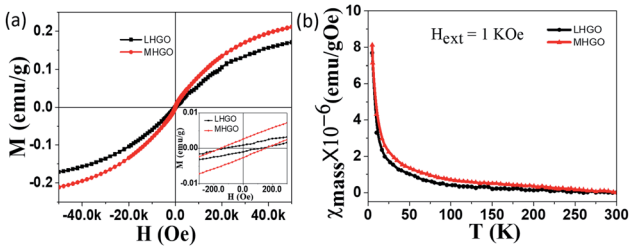

Fig. 4 Magnetic properties of as-prepared LHGO and MHGO measured by PPMS. (a) Typical M–H curve measured at 5 K. Inset is the enlarged part of the magnetization curve. (b) χ–T curve measured from 5 to 300 K under the extra field H = 1 kOe.

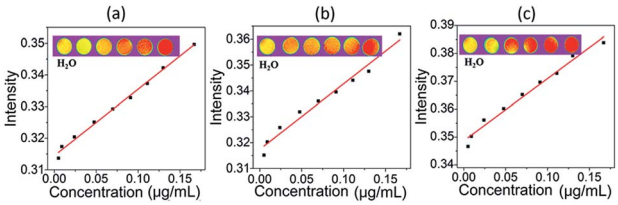

Fig. 5 (a), (b), (c) are magnetic properties of as-prepared GO, LHGO, and MHGO on 4.7 T MRI scanner, respectively. The upper part of figure is the T_1-weighted MR images of GO (a), LHGO (b), MHGO (c) in aqueous solutions at different concentrations.

Unlike GO, MHGO and LHGO behaved different magnetic properties. Fig. 4a showed the typical mass magnetization (M–H) curve of LHGO and MHGO measured at 5 K. The isothermal magnetization curve clearly showed hysteresis with a coercivity of ~151 Oe and ~118 Oe for MHGO and LHGO (inset of Fig. 4a), respectively, and saturation magnetization reaching 0.21 emu g^{-1}, 0.17 emu g^{-1} for MHGO and LHGO, respectively. Interestingly, the increase of magnetization from 0.14 and 0.17 to 0.21 emu g^{-1} was accompanied by the size and density of nanoholes on the nanosheets of GO increased. In the other hand, the increase of magnetization correlated with the number of dangling bonds on GO that was adjusted by the generating and increasing of nanoholes. Since the dangling bonds can generate localized magnetic moments, the distance between the magnetic moments decrease with the increased dangling bonds. It has been demonstrated that owing to the long distance between magnetic moments, graphene with low magnetization shows pure Curie-like paramagnetism.[45–47] And the magnetic coupling between magnetic moments is the preliminary existence of ferromagnetic ordering for GO. Thus, it can be assumed that nanoholes increased the amounts of dangling bonds on GO, and so lead to the enhancement of GO magnetism and the generation of GO ferromagnetism. Subsequently, the χ–T measurement of both MHGO and LHGO was performed and no T_c was found from 5 K to 300 K (Fig. 4b), implying the T_c of the MHGO and LHGO was above the temperature of 300 K.

In order to further prove the magnetic properties of as-prepared samples, magnetic resonance imaging (MRI) of as-prepared samples was applied. Typical T_1-weighted MR images recorded for GO, LHGO, and MHGO in aqueous solutions clearly demonstrated all the samples had excellent T_1 relaxation properties (Fig. 5), and the linear correlations were very strong between the sample concentrations and the $1/T_1$.

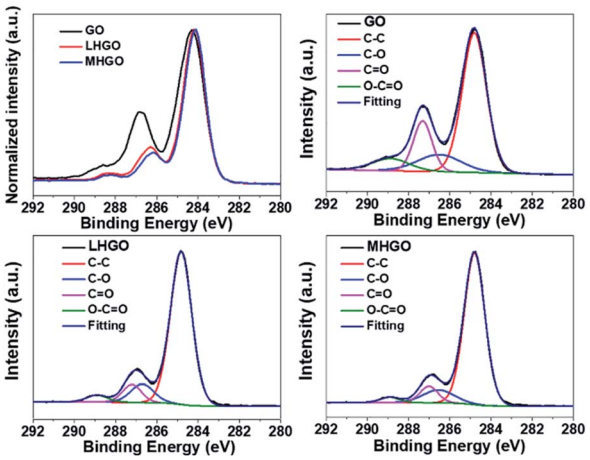

Fig. 6 High-resolution C1s XPS patterns of GO, LHGO, and MHGO, respectively.

The results in Fig. 5 also indicated that GO nanosheets exhibited a regularly enhancement in MRI signals. The transverse relaxivities (R_1) of GO, LHGO, and MHGO were measured to be 210, 223 and 253 mg mL^{-1} S^{-1} on the 4.7 T MRI scanner by the x-axis of the GO concentration (mg mL^{-1}) in Table 1. From Table 1, R_1 values of GO samples were enhanced with the increasing amount of nanoholes. The possible reason may be that the increasing amount of nanoholes resulted in the dangling bonds increasing and oxygen-containing groups decreasing.

To accurately investigate the content of the hydrophilic groups on the as-prepared GO, LHGO, and MHGO, high-resolution C1s XPS spectra were recorded for as-prepared samples (Fig. 6 and Table 2). In comparison, although the C1s XPS spectra of LHGO and MHGO exhibited the same oxygen functional groups, their peak intensities were lower than those in GO. The results indicated the partial removal of the oxygen-containing functional groups in HGO. In addition, MHGO removed little more oxygen-containing functional groups than LHGO. The content of oxygen-containing functional groups decreased with the increase of nanoholes on GO. In addition, it has been reported that O contributed little to the increase of the magnetization.[45] Therefore, the enhancement of R_1 of GO was only related to the dangling bonds on GO.

FTIR was also used to characterize the functionalized groups of the as-prepared samples. As shown in Fig. 7, the absorption intensities of the HGO peaks at 2500–3700 cm^{-1} (–OH groups),

Table 1 The relaxation of GO nanosheets

Samples	Relaxivity (R_1)	R	Concentrations (mg mL^{-1})
GO	210.13	0.993	0.00498–0.167
LHGO	223.03	0.979	0.00498–0.167
MHGO	253.33	0.973	0.00498–0.167

Table 2 The peak area ratios (%) of C–C bonds and the oxygen-containing bonds for GO, LHGO, and MHGO

Samples	C–C (%)	C–O (%)	C=O (%)	O=C–O (%)
GO	61.1	13.6	17.1	8.2
LHGO	78.3	10.2	8.0	3.5
MHGO	79.8	10.0	7.6	2.6

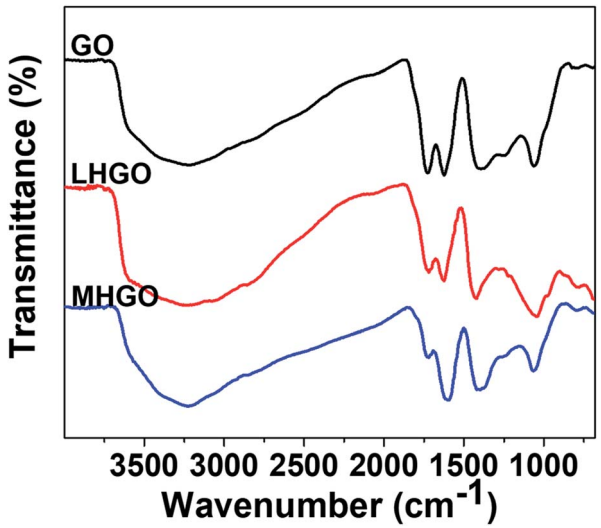

Fig. 7 FTIR spectra of as-prepared GO, LHGO and MHGO.

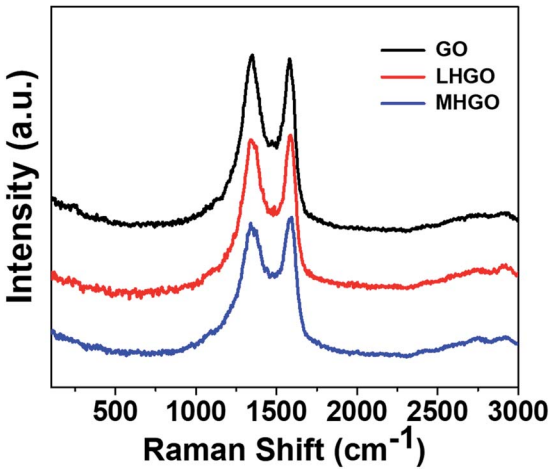

Fig. 9 Raman spectra of as-prepared GO, LHGO, and MHGO.

1730 cm^{-1}(C=O groups), and 1225 cm^{-1}(C–OH groups) were decreased compared to the intensity of corresponding group peaks of GO,[45] indicating the reduction of graphene sheets. Furthermore, the content of hydrophilic groups of MHGO decreased a little more than that of LHGO as the number of nanoholes on the GO surface increased, which was consistent with the corresponding XPS spectra (Fig. 6).

GO showed a strong peak at 230 nm in UV-vis spectrum, and the peak was blue-shifted as the density and size of nanoholes on the basal plane of GO increased (Fig. 8). Because the peak was aroused by π–π* transition of the sp^2 C of GO, the blue shift of the peak of HGO indicated that the presence of nanoholes on the GO nanosheets reduced the size of aromatic domains (sp^2 C) and so increased the proportion of sp^3 C in HGO. In addition, the peak at 230 nm of MHGO was more blue-shifted than LHGO, indicating that nanoholes on GO nanosheets reduced the proportion of sp^2 C and relatively increased the proportion of sp^3 C in GO. Therefore, the number of dangling bonds and/or chemical groups increased with the nanoholes on the GO raised. Combined with the magnetism, XPS, FTIR, it indicated that the amounts of dangling bonds increased with the number of nanoholes increased and could be adjusted by nanoholes on GO.

Raman spectroscopy can be used to characterize structural information of as-prepared materials.[48,49] Fig. 9 showed the Raman spectra of as-prepared GO, LHGO, and MHGO. The peaks around 1342 cm^{-1} and 1590 cm^{-1} correspond to the D and G bands of the carbon materials, respectively. It was observed that the I_D/I_G ratio was 1.02, 0.98, 0.95 for GO, LHGO, and MHGO, respectively. This suggested that the nanoholes on HGO sheets almost did not repair the aromatic domains of GO. The crystallite size calculated by the integrated intensity ratio of D and G peaks also indicated the nanoholes on the nanosheet of GO nearly did not restore its sp^2 structure.[50] Otherwise, the overall size of HGO nanosheets was almost unchanged compared to that of GO nanosheets while the amounts of functional groups decreased, so most of the nanoholes were formed at the position of the defects on the GO nanosheets.

In this experiment, we found that (1) the relative content of C–C bonds increased with the increased amounts of nanoholes on GO (Fig. 6 and Table 2), (2) the relative amount of C–C sp^2 should be decreased and the proportion of sp^3 C should be increased in GO with the nanoholes increased because the C–C bonds were broken due to the nanoholes initiation on the GO nanosheets, which had been proved by UV-vis spectra (Fig. 8), (3) the content of oxygen-containing functional groups decreased with the increasing nanoholes on GO (Fig. 8 and 9).

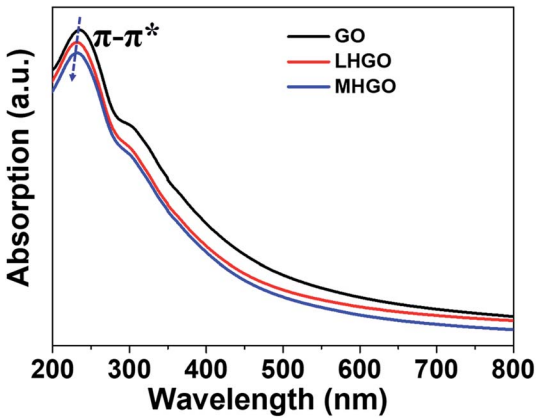

Fig. 8 UV-vis spectra of GO, LHGO and MHGO.

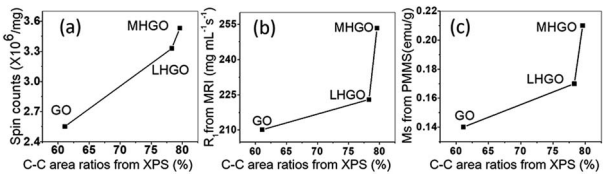

Fig. 10 The relations between C–C sp^3 bonds from XPS spectra and the spin counts in (a), relaxivities of R1 in (b) and magnetic properties in (c) of GO, LHGO and MHGO, respectively.

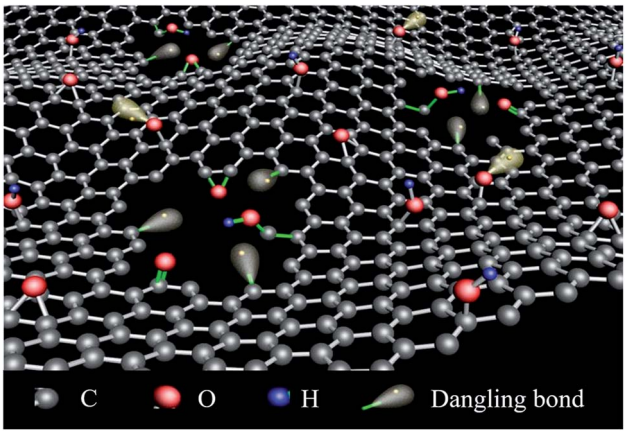

Fig. 11 The schematic diagram of HGO with different nanoholes and dangling bonds.

Therefore, the relative contents of C–C bonds from the XPS spectra could stand for the relative amounts of the dangling bonds on the GO. From Fig. 10, the relative contents of C–C sp^3 bonds had obviously positive correlation with the number of magnetic related properties, such as spins from ESR, relaxivities of R_1, and magnetic properties Ms of GO, LHGO, and MHGO. That indicated that the magnetism of GO could be adjusted by controlling the amounts of dangling bonds on GO.

It was also found that the introduction of nanoholes on nanosheets of GO by H_2O_2 mainly initiated within the oxygenic defect regions, leading to the removal of oxygenated carbon atoms (Fig. 6 and 7) and part sp^2 carbon atoms and so generate carbon vacancies and gradually extend into nanoholes in GO. The removal would bring various edges and defect sites with dangling bonds on GO.[43] On the other hand, the generation of nanoholes in the basal plane of GO could bring new edges and so produce dangling bonds in where there was no chemical group (Fig. 11). Therefore, the amount of dangling bonds on GO could be adjusted by controlling the size and density of nanoholes on GO. Since the dangling bonds have an important contribution to the edge magnetism of graphene,[39] the magnetism of GO could be regulated by nanoholes on GO.[51]

It has been confirmed that GO exhibited pure Curie-like paramagnetism due to the long distance between magnetic movements. Nanoholes could generate dangling bonds and so increased density of dangling bonds which led to the shorter distance between magnetic movements, resulting in enhancing magnetic coupling that made GO ferromagnetic. In addition, the ferromagnetism increased more in MHGO than LHGO for the more density magnetic movements, so there was stronger magnetic coupling between the magnetic movements induced by more dangling bonds on MHGO than on LHGO nanosheets.

Conclusion

In conclusion, we have taken advantage of holey graphene oxide to control and adjust magnetism of GO. The number of nanoholes on GO (MHGO and LHGO) was controlled by precisely controlling etching conditions for GO. The amounts of dangling bonds on GO could be adjusted by the number of nanoholes on GO nanosheets and they could be quantitatively measured. The increased dangling bonds originated in the increasing nanoholes on the GO nanosheets converted paramagnetism GO to ferromagnetism with enhancing magnetic coupling between the spin units. Therefore, the magnetic property of GO could be adjusted by varied number of holes on the GO through etching. The present work opens new possibilities way for further application of GO in spintronic devices, which can further expand the application of GO in nanoelectronic devices.[52]

Conflicts of interest

The authors declare that there are no conflicts of interest.

Acknowledgements

This work was supported financially by the National Key Research and Development Program of China (2018YFA0703504), National Basic Research Program of China (2016YFA0203200, 2015CB930104), National Natural Science Foundation of China (21971242, U1632113, 21402202, 11505191, 51571185, 31571028, 11705211), Beijing Natural Science Foundation (2182089), and Young Scientist Innovative Foundation of IHEP (No. E05469U2, Y95461C).

References

1 A. K. Geim and K. S. Novoselov, The rise of graphene, *Nat. Mater.*, 2007, **6**(3), 183–191.
2 G. Yang, L. H. Li, W. B. Lee and M. C. Ng, Structure of graphene and its disorders: a review, *Sci. Technol. Adv. Mater.*, 2018, **19**(1), 613–648.
3 R. L. Cui, J. Li, H. Huang, M. Y. Zhang, X. H. Guo, Y. A. Chang, M. Li, J. Q. Dong, B. Y. Sun and G. M. Xing, Novel carbon nanohybrids as highly efficient magnetic resonance imaging contrast agents, *Nano Res.*, 2015, **8**(4), 1259–1268.
4 L. Z. Li, R. Qin, H. Li, L. L. Yu, Q. H. Liu, G. F. Luo, Z. X. Gao and J. Lu, Functionalized Graphene for High-Performance Two-Dimensional Spintronics Devices, *ACS Nano*, 2011, **5**(4), 2601–2610.
5 N. Tombros, C. Jozsa, M. Popinciuc, H. T. Jonkman and B. J. van Wees, Electronic spin transport and spin precession in single graphene layers at room temperature, *Nature*, 2007, **448**(7153), 571–574.
6 M. A. Akhukov, S. J. Yuan, A. Fasolino and M. I. Katsnelson, Electronic, magnetic and transport properties of graphene ribbons terminated by nanotubes, *New J. Phys.*, 2012, **14**, 123012–123023.
7 A. Y. S. Eng, H. L. Poh, F. Sanek, M. Marysko, S. Matejkova, Z. Sofer and M. Pumera, Searching for Magnetism in Hydrogenated Graphene: Using Highly Hydrogenated Graphene Prepared *via* Birch Reduction of Graphite Oxides, *ACS Nano*, 2013, **7**(7), 5930–5939.
8 L. Veyrat, A. Jordan, K. Zimmermann, F. Gay, K. Watanabe, T. Taniguchi, H. Sellier and B. Sacepe, Low-Magnetic-Field

Regime of a Gate-Defined Constriction in High-Mobility Graphene, *Nano Lett.*, 2019, **19**(2), 635–642.

9 A. Mallick, A. S. Mahapatra, A. Mitra, J. M. Greneche, R. S. Ningthoujam and P. K. Chakrabarti, Magnetic properties and bio-medical applications in hyperthermia of lithium zinc ferrite nanoparticles integrated with reduced graphene oxide, *J. Appl. Phys.*, 2018, **123**(5), 055103.

10 P. F. Chen, N. Li, X. Z. Chen, W. J. Ong and X. J. Zhao, The rising star of 2D black phosphorus beyond graphene: synthesis, properties and electronic applications, *2D Mater*, 2018, **5**(1), 014002.

11 J. W. Yi, S. B. Lee, D. G. Seong, S. K. Lee, K. H. Kim and O. O. Park, Effect of iron-deposited graphene oxides on the electromagnetic wave absorbing property of polymer composite films with Fe-based hollow magnetic fibers for near-field applications, *J. Alloys Compd.*, 2016, **663**, 196–203.

12 H. Overweg, H. Eggimann, M. H. Liu, A. Varlet, M. Eich, P. Simonet, Y. J. Lee, K. Watanabe, T. Taniguchi, K. Richter, V. I. Fal'ko, K. Ensslin and T. Ihn, Oscillating Magnetoresistance in Graphene p–n Junctions at Intermediate Magnetic Fields, *Nano Lett.*, 2017, **17**(5), 2852–2857.

13 J. W. Bai, X. Zhong, S. Jiang, Y. Huang and X. F. Duan, Graphene nanomesh, *Nat. Nanotechnol.*, 2010, **5**(3), 190–194.

14 Y. X. Xu, C. Y. Chen, Z. P. Zhao, Z. Y. Lin, C. Lee, X. Xu, C. Wang, Y. Huang, M. I. Shakir and X. F. Duan, Solution Processable Holey Graphene Oxide and Its Derived Macrostructures for High-Performance Supercapacitors, *Nano Lett.*, 2015, **15**(7), 4605–4610.

15 A. S. Fedorov, Z. I. Popov, D. A. Fedorov, N. S. Eliseeva, M. V. Serjantova and A. A. Kuzubov, DFT investigation of the influence of ordered vacancies on elastic and magnetic properties of graphene and graphene-like SiC and BN structures, *Phys. Status Solidi B*, 2012, **249**(12), 2549–2552.

16 N. S. Eliseeva, A. A. Kuzubov, S. G. Ovchinnikov, M. V. Serzhantova, F. N. Tomilin and A. S. Fedorov, Theoretical study of the magnetic properties of ordered vacancies in 2D hexagonal structures: Graphene, 2D-SiC, and h-BN, *JETP Lett.*, 2012, **95**(11), 555–559.

17 G. Z. Magda, X. Z. Jin, I. Hagymasi, P. Vancso, Z. Osvath, P. Nemes-Incze, C. Y. Hwang, L. P. Biro and L. Tapaszto, Room-temperature magnetic order on zigzag edges of narrow graphene nanoribbons, *Nature*, 2014, **514**(7524), 608–611.

18 P. Lu, R. L. Zhou, W. L. Guo and X. C. Zeng, Amide Functionalization of Graphene and Carbon Nanotubes: Coverage- and Pattern-Dependent Electronic and Magnetic Properties, *J. Phys. Chem. C*, 2012, **116**(25), 13722–13730.

19 W. Fa and J. Zhou, Electronic and magnetic properties of chevron-type graphene nanoribbon edge-terminated by oxygen atoms, *Phys. Lett. A*, 2012, **377**(1–2), 112–117.

20 G. Eda and M. Chhowalla, Chemically Derived Graphene Oxide: Towards Large-Area Thin-Film Electronics and Optoelectronics, *Adv. Mater.*, 2010, **22**(22), 2392–2415.

21 J. Lu, Y. Bao, C. L. Su and K. P. Loh, Properties of Strained Structures and Topological Defects in Graphene, *ACS Nano*, 2013, **7**(10), 8350–8357.

22 L. Salemi, A. Lherbier and J. C. Charlier, Spin-dependent properties in zigzag graphene nanoribbons with phenyl-edge defects, *Phys. Rev. B*, 2018, **98**(21), 214204.

23 T. Tang, F. C. Liu, Y. Liu, X. Y. Li, Q. H. Xu, Q. Feng, N. J. Tang and Y. W. Du, Identifying the magnetic properties of graphene oxide, *Appl. Phys. Lett.*, 2014, **104**(12), 123104.

24 T. Taniguchi, H. Yokoi, M. Nagamine, H. Tateishi, A. Funatsu, K. Hatakeyama, C. Ogata, M. Ichida, H. Ando, M. Koinuma and Y. Matsumoto, Correlated Optical and Magnetic Properties in Photoreduced Graphene Oxide, *J. Phys. Chem. C*, 2014, **118**(48), 28258–28265.

25 K. Bagani, M. K. Ray, B. Satpati, N. R. Ray, M. Sardar and S. Banerjee, Contrasting Magnetic Properties of Thermally and Chemically Reduced Graphene Oxide, *J. Phys. Chem. C*, 2014, **118**(24), 13254–13259.

26 P. Blonski, J. Tucek, Z. Sofer, V. Mazanek, M. Petr, M. Pumera, M. Otyepka and R. Zboril, Doping with Graphitic Nitrogen Triggers Ferromagnetism in Graphene, *J. Am. Chem. Soc.*, 2017, **139**(8), 3171–3180.

27 D. Lee, I. Nekrashevich, H. J. Lee, C. Dannangoda, K. S. Martirosyan, T. R. Lee and D. Litvinov, Spin-Glass Behavior in Graphene Oxide Powders Induced by Nonmagnetic Sodium Sulfate, *Chem. Mater.*, 2017, **29**(9), 3873–3882.

28 J. C. Li, N. Friedrich, N. Merino, D. G. de Oteyza, D. Pena, D. Jacob and J. I. Pascual, Electrically Addressing the Spin of a Magnetic Porphyrin through Covalently Connected Graphene Electrodes, *Nano Lett.*, 2019, **19**(5), 3288–3294.

29 Q. Li, H. P. Lin, R. T. Lv, M. Terrones, L. F. Chi, W. A. Hofer and M. H. Pan, Locally Induced Spin States on Graphene by Chemical Attachment of Boron Atoms, *Nano Lett.*, 2018, **18**(9), 5482–5487.

30 L. Gragnaniello, F. Paschke, P. Erler, P. Schmitt, N. Barth, S. Simon, H. Brune, S. Rusponi and M. Fonin, Uniaxial 2D Superlattice of Fe-4 Molecular Magnets on Graphene, *Nano Lett.*, 2017, **17**(12), 7177–7182.

31 Z. Y. Zeng, X. Huang, Z. Y. Yin, H. Li, Y. Chen, H. Li, Q. Zhang, J. Ma, F. Boey and H. Zhang, Fabrication of Graphene Nanomesh by Using an Anodic Aluminum Oxide Membrane as a Template, *Adv. Mater.*, 2012, **24**(30), 4138–4142.

32 J. Yang, M. Z. Ma, L. Q. Li, Y. F. Zhang, W. Huang and X. C. Dong, Graphene nanomesh: new versatile materials, *Nanoscale*, 2014, **6**(22), 13301–13313.

33 Y. Lin, K. A. Watson, J. W. Kim, D. W. Baggett, D. C. Working and J. W. Connell, Bulk preparation of holey graphene *via* controlled catalytic oxidation, *Nanoscale*, 2013, **5**(17), 7814–7824.

34 G. P. Kotchey, B. L. Allen, H. Vedala, N. Yanamala, A. A. Kapralov, Y. Y. Tyurina, J. Klein-Seetharaman, V. E. Kagan and A. Star, The Enzymatic Oxidation of Graphene Oxide, *ACS Nano*, 2011, **5**(3), 2098–2108.

35 O. Akhavan, Graphene Nanomesh by ZnO Nanorod Photocatalysts, *ACS Nano*, 2010, **4**(7), 4174–4180.

36 X. Zhao, C. M. Hayner, M. C. Kung and H. H. Kung, Flexible Holey Graphene Paper Electrodes with Enhanced Rate

Capability for Energy Storage Applications, *ACS Nano*, 2011, **5**(11), 8739–8749.

37 H. K. Kim, S. M. Bak, S. W. Lee, M. S. Kim, B. Park, S. C. Lee, Y. J. Choi, S. C. Jun, J. T. Han, K. W. Nam, K. Y. Chung, J. Wang, J. G. Zhou, X. Q. Yang, K. C. Roh and K. B. Kim, Scalable fabrication of micron-scale graphene nanomeshes for high-performance supercapacitor applications, *Energy Environ. Sci.*, 2016, **9**(4), 1270–1281.

38 J. Sun, S. E. Lowe, L. J. Zhang, Y. Z. Wang, K. L. Pang, Y. Wang, Y. L. Zhong, P. R. Liu, K. Zhao, Z. Y. Tang and H. J. Zhao, Ultrathin Nitrogen-Doped Holey Carbon@Graphene Bifunctional Electrocatalyst for Oxygen Reduction and Evolution Reactions in Alkaline and Acidic Media, *Angew. Chem. Int. Ed.*, 2018, **57**(50), 16511–16515.

39 M. A. Akhukov, A. Fasolino, Y. N. Gornostyrev and M. I. Katsnelson, Dangling bonds and magnetism of grain boundaries in graphene, *Phys. Rev. B*, 2012, **85**(11), 115407.

40 T. J. Lyon, J. Sichau, A. Dorn, A. Centeno, A. Pesquera, A. Zurutuza and R. H. Blick, Probing Electron Spin Resonance in Monolayer Graphene, *Phys. Rev. Lett.*, 2017, **119**(6), 066802.

41 B. Dora, F. Muranyi and F. Simon, Electron spin dynamics and electron spin resonance in graphene, *Europhys. Lett.*, 2010, **92**(1), 17002.

42 D. Izci, C. Dale, N. Keegan and J. Hedley, The Construction of a Graphene Hall Effect Magnetometer, *IEEE Sens. J.*, 2018, **18**(23), 9534–9541.

43 S. Pisana, P. M. Braganca, E. E. Marinero and B. A. Gurney, Tunable Nanoscale Graphene Magnetometers, *Nano Lett.*, 2010, **10**(1), 341–346.

44 M. Sepioni, R. R. Nair, S. Rablen, J. Narayanan, F. Tuna, R. Winpenny, A. K. Geim and I. V. Grigorieva, Limits on Intrinsic Magnetism in Graphene, *Phys. Rev. Lett.*, 2010, **105**(20), 207205.

45 Y. Liu, N. J. Tang, X. G. Wan, Q. Feng, M. Li, Q. H. Xu, F. C. Liu and Y. W. Du, Realization of ferromagnetic graphene oxide with high magnetization by doping graphene oxide with nitrogen, *Sci. Rep.*, 2013, **3**, 2566.

46 M. Kan, J. Zhou, Q. Sun, Q. Wang, Y. Kawazoe and P. Jena, Tuning magnetic properties of graphene nanoribbons with topological line defects: From antiferromagnetic to ferromagnetic, *Phys. Rev. B*, 2012, **85**(15), 155450.

47 B. Genorio, Z. W. Peng, W. Lu, B. K. P. Hoelscher, B. Novosel and J. M. Tour, Synthesis of Dispersible Ferromagnetic Graphene Nanoribbon Stacks with Enhanced Electrical Percolation Properties in a Magnetic Field, *ACS Nano*, 2012, **6**(11), 10396–10404.

48 Y. Henni, H. P. O. Collado, K. Nogajewski, M. R. Molas, G. Usaj, C. A. Balseiro, M. Orlita, M. Potemski and C. Faugeras, Rhombohedral Multilayer Graphene: A Magneto-Raman Scattering Study, *Nano Lett.*, 2016, **16**(6), 3710–3716.

49 S. Berciaud, M. Potemski and C. Faugeras, Probing Electronic Excitations in Mono- to Pentalayer Graphene by Micro Magneto-Raman Spectroscopy, *Nano Lett.*, 2014, **14**(8), 4548–4553.

50 A. C. Ferrari, Raman spectroscopy of graphene and graphite: Disorder, electron-phonon coupling, doping and nonadiabatic effects, *Solid State Commun.*, 2007, **143**(1–2), 47–57.

51 E. J. G. Santos, A. Ayuela and D. Sanchez-Portal, Universal magnetic properties of sp(3)-type defects in covalently functionalized graphene, *New J. Phys.*, 2012, **14**, 043022.

52 B. Barnes, I. Elkholy, N. Bane, J. Derickson, X. Guo and K. Das, Laser scribed graphene/polymer composites: A possible verification of carbon nano-coil inductors, *Curr. Appl. Phys.*, 2020, 1567–1739.